https://doi.org/10.1016/j.jweia.2021.104714

Impact of wind turbulence on thermal perception in the urban microclimate

Yichen Yu[a], Richard de Dear[a]*, Kapil Chauhan[b], Jianlei Niu[b, c]

[a] School of Architecture, Design and Planning, The University of Sydney, NSW, Australia

[b] Centre for Wind, Waves and Water, School of Civil Engineering, The University of Sydney, NSW, Australia

[c] Department of Building Services Engineering, The Hong Kong Polytechnic University, Hung Hom, Kowloon, Hong Kong

*Corresponding author: richard.dedear@sydney.edu.au

Abstract

Ongoing urbanization has led to complexities in the urban terrain, increasing roughness length within the atmospheric surface layer, and introduced highly turbulent wind flow at pedestrian height. This research aims to explicitly examine the effect of wind flow turbulence on thermal perception under outdoor conditions. A wind tunnel with passive grid was used to introduce turbulence into simulated wind conditions. Thermal physiological (skin temperature) and perceptual (questionnaire) responses were collected from 20 college-age subjects during the exposures to various simulated urban wind conditions. Results confirm that increased turbulence intensity enhances perceived coolness by reducing the skin temperature. We updated the convective heat transfer coefficient in a numerical skin thermoreceptor model and also Gagge's two-node thermophysiological model so that they both reflect more accurately the effects of turbulence intensity on skin temperature. Skin temperatures simulated with the modified models were in good agreement with experimental observations, and corrected the un-modified model's 30% and 50% underestimation of mean skin temperature decrement for standing and cycling conditions respectively. These findings contribute to the broader goal of a thermal comfort model for application to urban microclimate.

Keywords: Wind; Turbulence intensity; Human subject experiment; Outdoor thermal comfort; Urban microclimate

1. Introduction

A sedentary lifestyle negatively impacts health, increasing the risk of cardiovascular diseases, diabetes, and obesity (Godbey, 2009). To compensate for diminished activity, communities are encouraged to spend more time engaged in outdoor activities. However, in

warm-to-hot climate zones where the rate of urbanisation is greatest, the urban heat island effect not only suppresses outdoor activities, but also deters citizens from walking to everyday destinations – shops, public transport hubs, and schools (Asimakopoulus & Santamouris, 2012). City designers, landscape architects, and engineers efforts to manage urban warming are focusing on performance testing various cooling strategies including artificial and natural shading (Lin et al., 2013) and enhancing air movement between buildings (Xie et al., 2018).

Compared with retrofitting environmental remediation based user feedback, it would be more efficient to design urban cooling strategies in the planning phase. Predictive thermal comfort models represent a useful tool in this endeavour. Such models link urban microclimatic characteristics to pedestrians' thermal perceptions, usually expressed on a 7-point thermal sensation scale (-3=cold, -2=cool, -1=slightly cool, 0=neutral, 1=slightly warm, 2=warm, 3=hot) (ASHRAE, 2017). Thermal environmental parameters (i.e., air temperature, mean radiant temperature, relative humidity, wind velocity), taken together with expected clothing insulation and activity intensity are the main inputs to a thermophysiological model that mathematically describes the heat exchanges at the body's surface, inside the body (passive system), and the thermal regulation process (active system) that those effects in the passive system would induce. Based on the calculated physiological parameters, thermal sensation model can then predict people's thermal perception.

Substantive improvements have been made since the simple two-node thermoregulatory model was first developed half a century ago (Stolwijk, 1971) in two distinct directions. First is the anatomy of the body, which has evolved from the simplistic single sphere of the two-node model (Gagge, 1971; Givoni & Goldman, 1972) into a multi-segment humanoid form with each segment comprising four layers: skin, fat, muscle, and core, each with its own thermal properties (Stolwijk, 1971). The second major evolution in numerical thermal regulation models related to the movement of blood between these multiple nodes, upgraded from a constant-temperature central blood compartment to an intricate system of arteries and veins capable of simulating counter-current heat exchanges between blood and the tissues through which it flows (Huizenga et al., 2001a; Kingma, 2012; Kingma et al., 2012; Zhang et al., 2001).

Despite refinements in the active system the heat exchanges between the passive system and its thermal environment remain oversimplified, ignoring the highly turbulent condition of the atmospheric boundary layer. Wind is represented by mean velocity only, with its fluctuating characteristics being filtered out. However, experimental (i.e. wind tunnel testing, field measurement) and numerical simulation studies (Assimakopoulos et al., 2003; Niachou et al., 2008; Oke, 1987; Stathopoulos, 2006; Scaperdas & Colvile, 1999) have confirmed the complex flow characteristics of the pedestrian-level wind environment. In the urban canopy layer, wind is easily governed by terrain surface characteristics and the immediate surroundings. Therefore, the unrealistic characterisation of air flowing over the surface of contemporary thermoregulation models may be one of the explanations of a persistent discrepancy between comfort model predictions and field observations (Xie et al., 2018; Xie et al., 2020).

While turbulence effects have not yet been incorporated into numerical thermoregulation models, they have long been recognised in the context of human perception of draught, defined as unwanted local cooling, in indoor settings (Fanger et al., 1988).The statistical draft risk model (Fanger et al., 1988) predicts the percentage of dissatisfaction caused by draught *PD*, as a function of the air temperature T_a, mean air velocity v, and the turbulence intensity *TI* of the air flow.

More recently research attention has shifted away from unpleasant draft effects in cool-to-neutral thermal environments (negative alliesthesia) towards the pleasant breeze effects of airflow in warm-than-neutral environments (Xia et al., 2000), termed positive alliesthesia (Huang et al., 2012; Parkinson & de Dear, 2016; Tanabe & Kimura, 1989; Zhou et al., 2010).

Among those studies which not only collected the subjective responses but also measured the skin temperature simultaneously, Parkinson and de Dear (2016) found that the frequency and amplitude of skin temperature fluctuation followed the pattern of air movement. Fanger et al. (1988) also long maintained the importance of fluctuations in skin temperature in eliciting sensations of draft discomfort, which is simply a synonym for negative alliesthesia.

But despite these significant research efforts into wind turbulence effects on subjective thermal comfort, its effect on convective heat loss has not been included in the exiting thermal regulation models. Mayer (1987) first to connected turbulence intensity to convective heat transfer at the skin surface, measuring it indirectly through the thermal boundary layer around an artificially heated manikin head, with the turbulence intensity ranging from 14% to 55% at mean wind velocity below 0.5 m/s. The experimental results proved that convective heat loss increases with turbulence intensity. His manikin studies were followed by a series of human subject experiments, with skin temperature differences investigated at average wind speeds between 0.1 m/s and 0.6 m/s and turbulence levels between 15% and 70%. Griefahn et al.'s (2000) experimental findings indicated that with a velocity range from still air up to 0.5 m/s the skin temperature differences between turbulence levels were almost indistinguishable from measurement error. Wang et al. (2011) suggested that the variation of skin temperature reduction at local sites only become noticeable between different turbulence intensities (15% and 30%) when the mean wind velocity exceeded 0.3 m/s. However, the highest wind speed been tested in the previous studies (1m/s) was far too low compared to typical outdoor pedestrian-level wind conditions.

Meanwhile, a recent study in which a thermal manikin was exposed to an outdoor air velocity range (0.7 to 6.9 m/s) confirmed that ignoring turbulence intensity of 30% resulted in convective heat transfer at the manikin's skin surface being underestimated by as much as 50% (Yu et al., 2020). Discrepancies of this magnitude emphasise that the effects of turbulence intensity cannot be dismissed as negligible, and therefore should be incorporated into contemporary thermal regulation models and their associated comfort predictions.

This study aims to verify the recent manikin-derived convective heat transfer coefficient formula, using physiological and psychological responses collected from the human subjects, tested under diverse combinations of metabolic rate, wind speed, and wind direction.

2. Materials and methods

The experiments were conducted in the Boundary Layer Wind Tunnel (BLWT) in the School of Civil Engineering at The University of Sydney. The tunnel is 20 m long, 2.5 m wide and 2 m high. The incoming air velocity was controlled through the rotational speed of the wind tunnel fan, and a coarse grid at the inlet (Fig.1a, see Yu et al., 2020 for a detailed description of the facility)was used to simulate outdoor urban wind environments with realistic turbulence intensity ranges (Zou et al., 2021). The wind speed at the test section equilibrated within 5 s after the wind tunnel fan was turned on. Vertically averaged turbulence intensity across the occupied zone (0.1-1.7 m) was approximately 35% for the high turbulence intensity measurements (*TI*-high), with the participant stood at 2.5m downwind of the grid system; and 17% for the low turbulence intensity measurements (*TI*-low) (Fig. 1c), with the distance increased to 5 m. We plotted the power spectral density of the 3-min measurement data against the frequency in a log-log scale in Fig.1d, which presents the results at 1.1 m height above the ground. It is seen in Fig. 1d that, the wind speed frequency distribution was quite close to each other. In the high-frequency band (10^{-2} Hz – 10^{0} Hz) where the airflow produces the strongest cooling effect, the measured wind spectra remain stable, which is different from natural wind that follows 1/ frequency decay rate (Zhao et al., 2006).

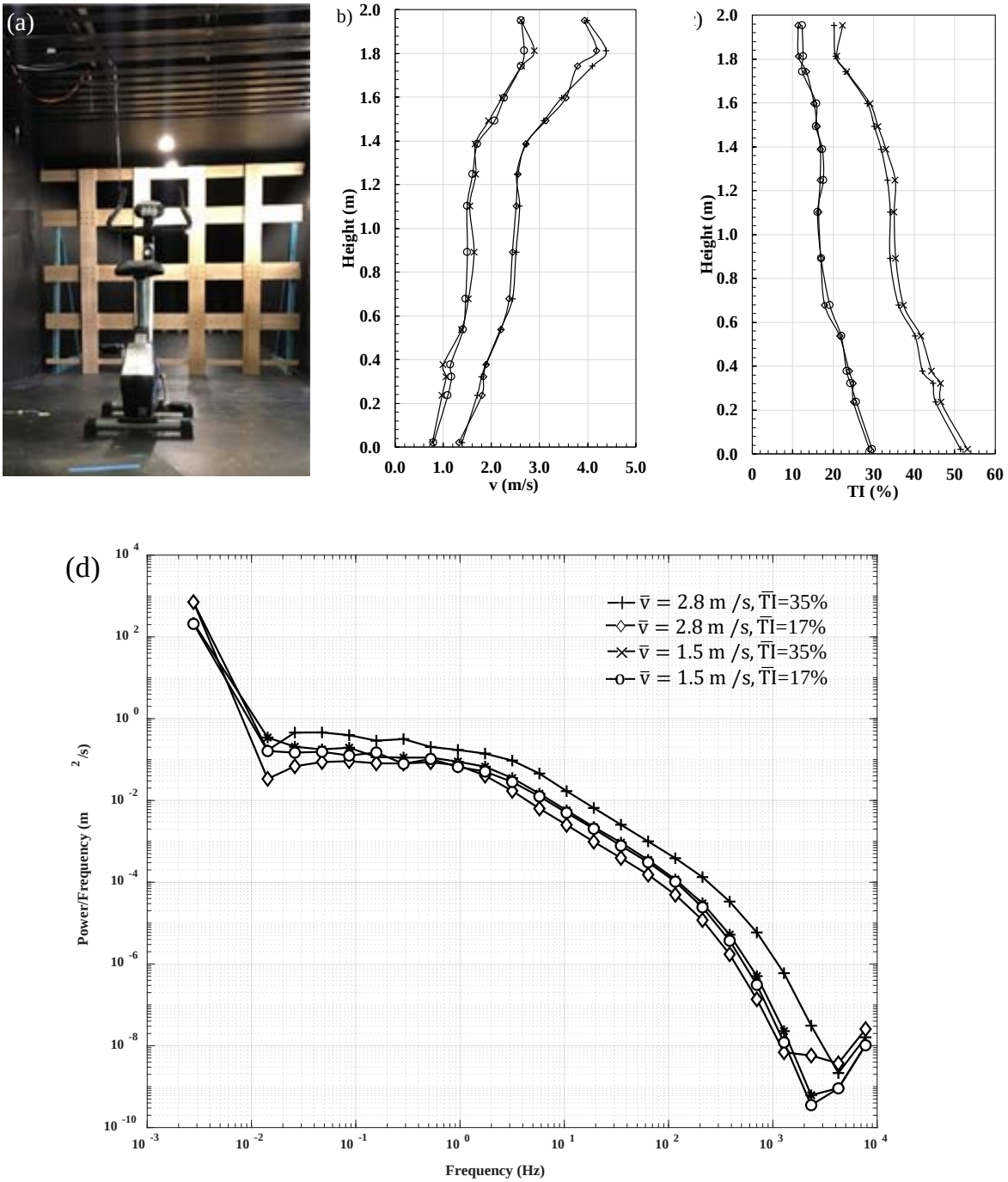

Fig.1. (a) placement of the ergometer for cycling wind, (b) velocity profile, (c) wind turbulence profile, and (d) power spectral density in the test section ("cross" represents $\bar{v}$=2.8 m/s, $\overline{TI}$= 35%, "diamond" represents $\bar{v}$=2.8 m/s, $\overline{TI}$=17%, "star" represents $\bar{v}$=1.5 m/s, $\overline{TI}$= 35%, "circle" represents $\bar{v}$=1.5 m/s, $\overline{TI}$= 17%).

Air temperature and relative humidity were measured using 'iButton' sensors (Onsolution, Thermochron, TCS) positioned throughout the occupied zone of the wind tunnel's working section. During the three-week experimental campaign air temperature and relative humidity inside the wind tunnel ranged from 25.9-28.7 °C, and 49-62% respectively, they were

relatively stable throughout each sequential pair of experiment (two different turbulence intensity levels).

Twenty university students participated in the experiment (demographic anthropometric information shown in Table 1). They were required to wear typical summer clothing (short sleeve t-shirts, sports shorts, socks, and sneakers); and as such the clothing insulation was estimimted at around 0.35 clo (1 clo = 0.155 m^2 ℃/W) (ASHRAE, 2017).

Table 1 Demographic and anthropometric details of experimental subjects.

Gender	n	Age (years)	Height (cm)	Weight (kg)	BMI (kg/m^2)
Male	10	$\mathbf{23.4 \pm 2.8}$	$\mathbf{176.0 \pm 6.2}$	$\mathbf{72.6 \pm 7.9}$	$\mathbf{23.4 \pm 2.4}$
Female	10	$\mathbf{24.6 \pm 4.9}$	$\mathbf{163.2 \pm 6.4}$	$\mathbf{58.4. \pm 6.7}$	$\mathbf{22.0 \pm 3.4}$
All	20	$\mathbf{23.9 \pm 3.9}$	$\mathbf{169.0 \pm 9.0}$	$\mathbf{64.7. \pm 10.2}$	$\mathbf{22.6 \pm 2.9}$

Each participant came to the wind tunnel twice, and each visit included one standing test condition (A or D in Table 2) and one cycling test condition (B or C in Table 2). Each test condition was repeated at low and high turbulence intensity (randomly chosen from the sequence I or II) for 10-minute and was followed by a 15-minute break interval (Fig. 2). Only one subject took part in the experiment at each time.

Table 2 Four test conditions of the research design.

Condition	Wind velocity (m/s)	Wind direction	Activity
A	1.5	facing	standing
B	1.5	side on	cycling
C	2.8	facing	cycling
D	2.8	side on	standing

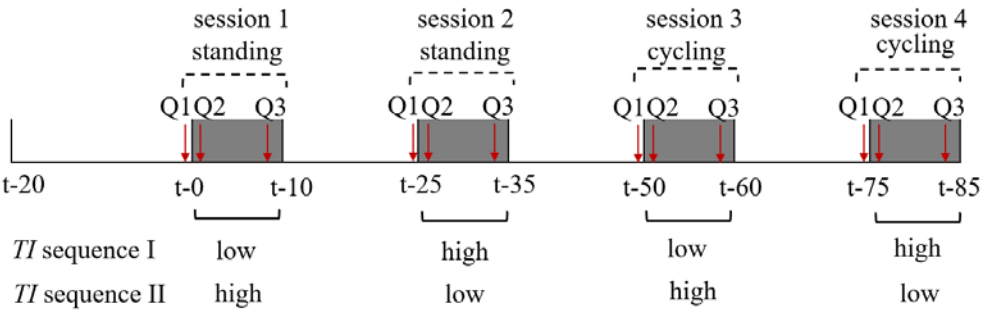

Fig. 2. Timeline of the research protocol

After arriving, participants first acclimatized themselves in a 23 ℃ air-conditioned chamber for 20 minutes, during which their resting heart rate (HR_{rest}) was measured through the Wahoo TICKR X H10 rate monitor – a soft textile strap fitted across the chest (Crouter et al., 2004). Their real-time heart rate was shown on the ergometer screen when cycling, with the cadence on the ergometer set to 60 rpm they were instructed to adjust the resistance to

maintain the real-time heart rate around the target value (HR), at which their metabolic rate would be the same (Yokota et al., 2008) as,

$$HR = HR_{\mathrm{rest}}\left(1 + \frac{(\mathrm{M}/58.1 * \mathrm{A_D} - 0.68}{5.73 - 0.052 * \mathrm{T_a}}\right) \quad (1)$$

Where,

$\mathrm{A_D}$ ($\mathrm{m^2}$) is the body surface area,

$\mathrm{T_a}$ (℃) is the ambient air temperature,

M (W/m2) is the target metabolic rate, set to 145, equals to 2.5 met.

In each test condition, the first questionnaire (Q1) ensured that subjects started with a *neutral* thermal sensation (i.e. zero on the ASHRAE 7-point scale). If that was not the case the subject was instructed to rest in the adjacent air-conditioned anteroom until neutrality was attained. After the wind tunnel fan was turned on, participants were requested to cast a thermal sensation vote the instant they felt the wind (Q2, t ~ 0.3 min). Thermal sensation votes were cast again in a stable condition at the end of each session (Q3, t = 8 min).

Skin temperatures at 14 body sites were continuously sampled at 1 Hz by thermocouples (±0.5 ℃ accuracy, 0.1 s time constant; Omega T-TT-36). The measurement points included left-face, forehead, neck, chest, back, abdomen, upper arms (covered by clothing), forearms, hands, left-front-thigh (not covered by clothing), and shin. The mean skin temperature was calculated as an eight-point weighted average (Gagge & Nishi, 1977), with around half of the body area, including chest, back, upper arm, forearm, and hand, on the leeward side, when the wind blows from the left in condition B and D. The absolute value of mean skin temperature might vary depending on different measurement points adopted but the relativity between different environmental exposure conditions should be unaffected by the choice of measurement sites.

$$\overline{\mathrm{T_{skin}}} = 0.07 * \mathrm{T_{forehead}} + 0.175 * \mathrm{T_{chest}} + 0.175 * \mathrm{T_{back}} + 0.07 * \mathrm{T_{R-upper-arm}} + 0.07 * \mathrm{T_{R-forearm}} + 0.05 * \mathrm{T_{R-hand}} + 0.19 * \mathrm{T_{L-thigh}} + 0.20 * \mathrm{T_{L-shin}} \quad (2)$$

A paired t-test was applied to the within-subject difference between thermal sensation votes and skin temperatures recorded at two turbulence levels (Hogg et al., 2010). The statistical analysis was performed with SPSS, and the significance level was set to 0.05 ($p < 0.05$).

3. Results and discussion

3.1 The effect of turbulence intensity on whole-body thermal perception

The participants were required to report their thermal sensation vote by filling in a questionnaire on their mobile device as soon as they felt the wind. This process took up to an average of 25 s over all the participants. Previous studies have suggested that the subjective sensation under a dynamic thermal stimulation is directly proportional to the impulse accumulated by the thermoreceptors within the first 20 s (de Dear et al., 1993). Therefore, we here adopted the skin temperature change within the first 20 s to correspond to the instantaneous thermal sensation vote (Q2). To compare the turbulence-induced psychological and physiological differences, we standardised the instantaneous and stable-state skin

temperature and thermal sensation vote (*TSV*) by calculating the difference from its nearest resting-state value as in Equations (3)-(6).

$$TSV_{\text{instant}} = TSV_{Q2} - TSV_{Q1} \quad (3)$$

$$T_{\text{skin\_instant}} = T\_skin_{t=0.3\text{min}} - T\_skin_{t=0} \quad (4)$$

$$TSV_{\text{stable}} = TSV_{Q3} - TSV_{Q1} \quad (5)$$

$$T_{\text{skin\_stable}} = T\_skin_{t=8\ \text{min}} - T\_skin_{t=0} \quad (6)$$

The increase of turbulence intensity could be reflected in a perceivable instantaneous thermal sensation difference for two facing conditions (**A** and **C**) (Table 3). While after 8-min exposure, the impact of different turbulence intensity on whole-body thermal sensation was more pronounced for two cycling conditions (**B** and **C)**. When subjects were standing, the cold sensation gradually increased within the 8-min exposure. For cycling, the heat generated by the muscles compensated the heat convected by the wind from the skin surfaces, leading to a thermal sensation near neutral at the end of the test; and the thermal sensation difference between two *TI* levels enlarged over time.

Table 3 Instantaneous and stable whole-body thermal sensation change (as defined in Equation 4 and 6) at the two turbulence intensity levels (mean ± standard deviation)

		Condition A	**Condition B**	**Condition C**	**Condition D**
$\boldsymbol{TSV_{\text{instant}}}$	TI-low	$(\mathbf{-1.3 \pm 0.4})$ *	$\mathbf{-1.3 \pm 1.2}$	$(\mathbf{-1.6 \pm 1.3})$ *	$\mathbf{-1.4 \pm 0.9}$
	TI-high	$(\mathbf{-1.8 \pm 0.8})$	$\mathbf{-1.5 \pm 1.3}$	$(\mathbf{-2.0 \pm 1.2})$	$\mathbf{-1.6 \pm 0.9}$
$\boldsymbol{TSV_{\text{stable}}}$	TI-low	$\mathbf{-1.6 \pm 0.6}$	$(\mathbf{0.4 \pm 1.6})$ *	$(\mathbf{0.2 \pm 1.7})$ *	$\mathbf{-2.0 \pm 0.9}$
	TI-high	$\mathbf{-1.9 \pm 1.0}$	$(\mathbf{0.0 \pm 1.1})$	$(\mathbf{-0.4 \pm 0.8})$	$\mathbf{-2.1 \pm 0.6}$

*significant difference according to t-test ($p < 0.05$) between two turbulence intensity levels

The body mean skin temperature decreased linearly within the first 20 s, and the decreasing trend flattened at the end of the test (Fig. 3). The most substantial decrement in skin temperature appeared in condition **C** - a combined outcome of higher wind speed and larger windward area. The turbulence-induced skin temperature difference is readily discernible from the space between two solid lines in Fig. 3. The stable state mean skin temperature ($\overline{T_{\text{skin\_stable}}}$) was at least 20% larger when the subject experienced a higher *TI* compared with a lower one for all four test conditions (Table 4).

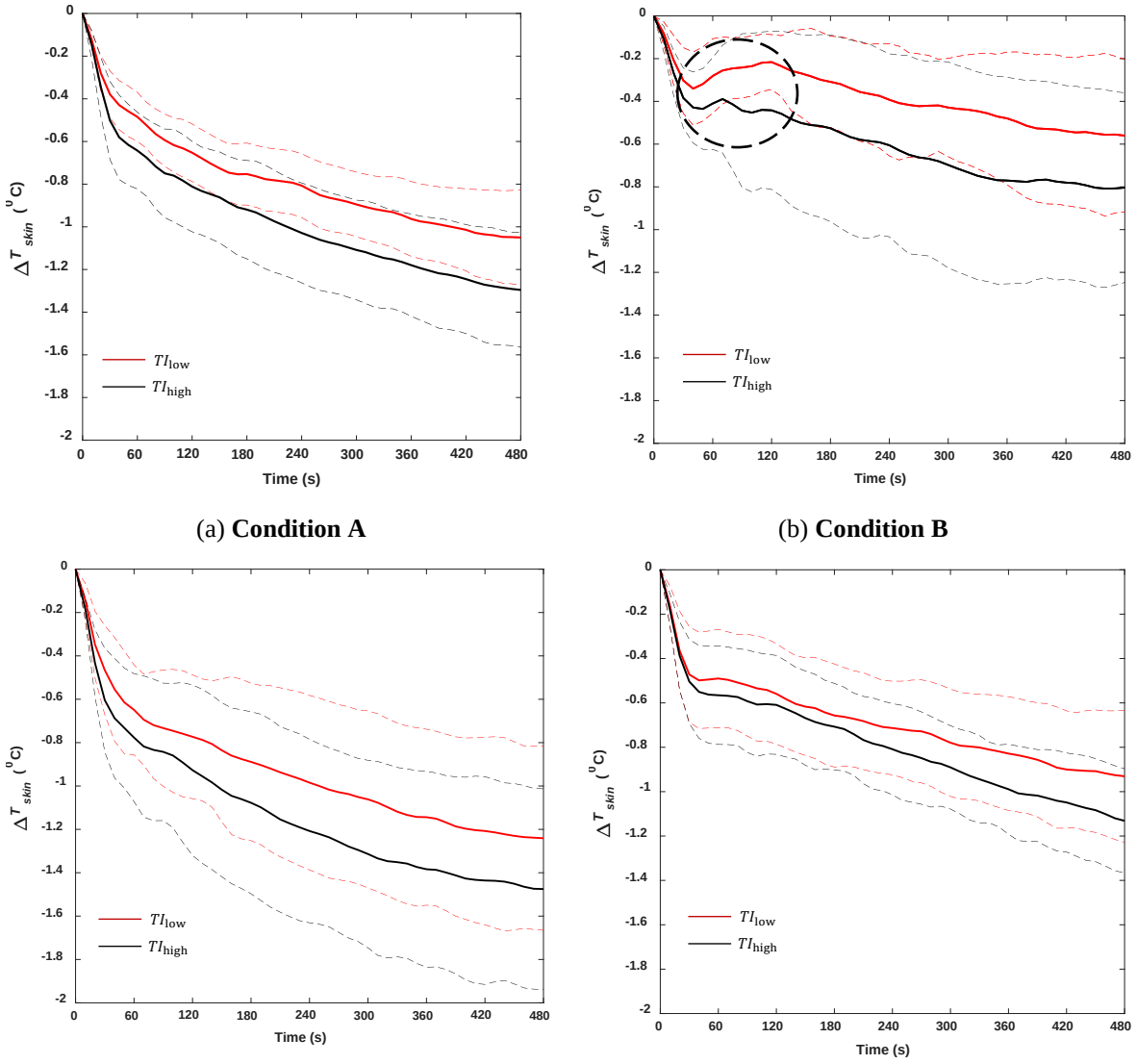

(a) **Condition A**

(b) **Condition B**

(c) **Condition C**

(d) **Condition D**

Fig.3. (a)-(d) Time series data of mean skin temperature for different test conditions, where the solid lines represent the mean value, and the dashed lines represent one standard deviation.

Table 4 Instantaneous and stable whole-body mean skin temperature change (as defined in Equation 5 and 7) at two turbulence intensity levels (mean ± standard deviation)

		Condition A	**Condition B**	**Condition C**	**Condition D**
$\overline{T_{skin\_instant}}$ (℃)	*TI*-low	(-0.38 ± 0.11)	-0.30 ± 0.15	(-0.47 ± 0.20)	-0.47 ± 0.22
	TI-high	(-0.50 ± 0.18)	-0.35 ± 0.14	(-0.60 ± 0.24)	-0.48 ± 0.18
$\overline{T_{skin\_stable}}$ (℃)	*TI*-low	(-1.05 ± 0.22)	(-0.56 ± 0.36)	(-1.24 ± 0.42)	(-0.95 ± 0.25)
	TI-high	(-1.30 ± 0.27)	(-0.80 ± 0.44)	(-1.48 ± 0.46)	(-1.16 ± 0.21)

*significant difference according to t-test ($p < 0.05$) between two turbulence intensity levels.

3.2 The effect of turbulence intensity on local body thermal perception

3.2.1 Skin temperature decrease

In this section we identify the local body segments exerting strongest influence on the whole-body thermal sensation and mean skin temperature. The configurations of body segments are presented in Fig. 4. From head to foot, body segments are forehead, left face, neck, chest, back, upper arms, forearms, hands, left front thigh and shin. To illustrate the turbulence-induced physiological and subjective differences, the left side of the body images depict local skin temperatures, and the corresponding local thermal sensations are shown on the right side. The instantaneous and steady-state responses are presented in the left and right column, respectively.

Instantaneously, a higher turbulence intensity mainly enhanced the degree of cooling on unclothed upper body parts, as reflected by the local skin temperature differences which achieved statistical significance. For the torso, which was covered under clothing, the turbulence-induced skin temperature change was less noticeable. When the wind approached from one side (left side of the body in this study), only those windward body segments sensed the difference in turbulence intensity.

Previous research suggested that the sensation of skin temperature change is a spatial summation of those thermoreceptor's responses elicited by the thermal stimulus (Darian-Smith & Johnson, 1977). The larger windward area when the subjects facing towards the wind resulted in a higher summative skin temperature difference, and therefore led to a more distinctive turbulence-induced cooling sensation in conditions **A** and **C**, compared with the rest two conditions of which the wind blows from the left side of the body.

By comparing **A** and **C**, **B** and **D**, wind velocity had a limited influence on instantaneous thermal perception difference at two turbulence levels. A similar finding was reported by Wang et al. (Wang et al., 2011), when subjects experienced two turbulence intensity levels (30% and 15%), the turbulence-induced skin temperature drop at the back of the neck remained constant at 0.5 ℃ for different wind velocities (0.3 m/s and 0.6 m/s).

At the end of the 8-min exposure, the turbulence-induced skin temperature and thermal sensation difference shifted from the upper limbs to the head and thigh (except for condition **D**, where the participants were standing side-on).

(a) Condition A

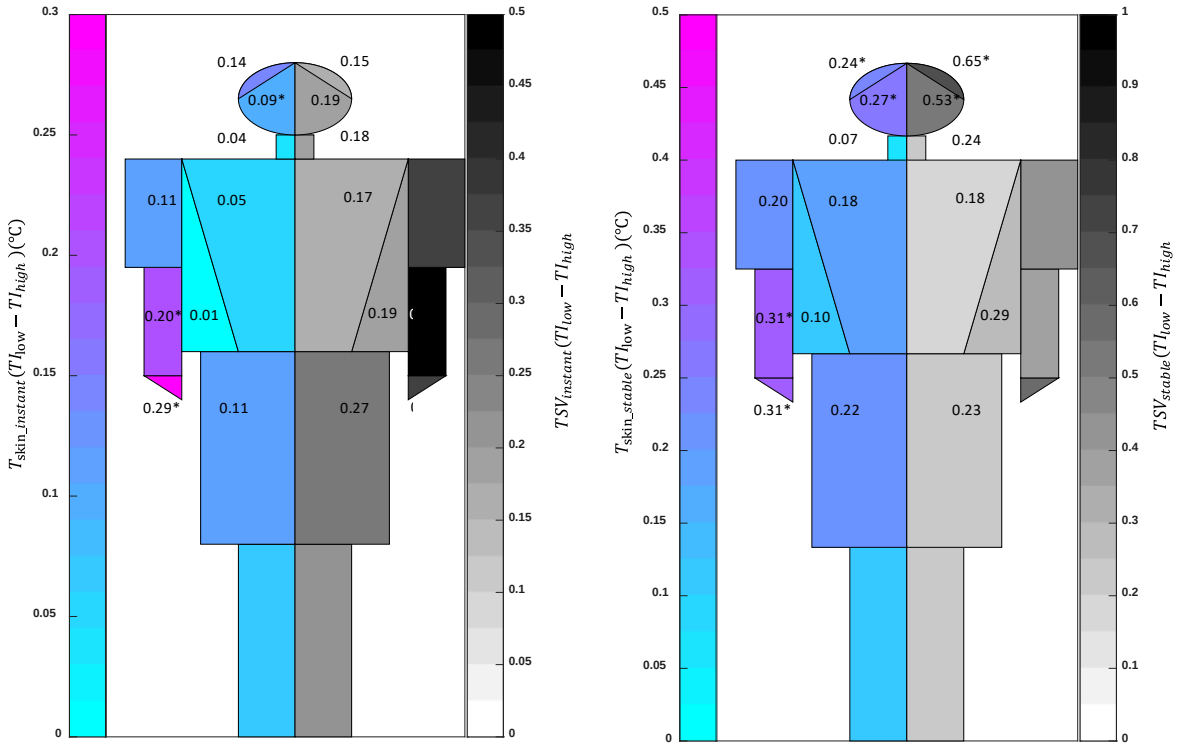

(b) Condition B

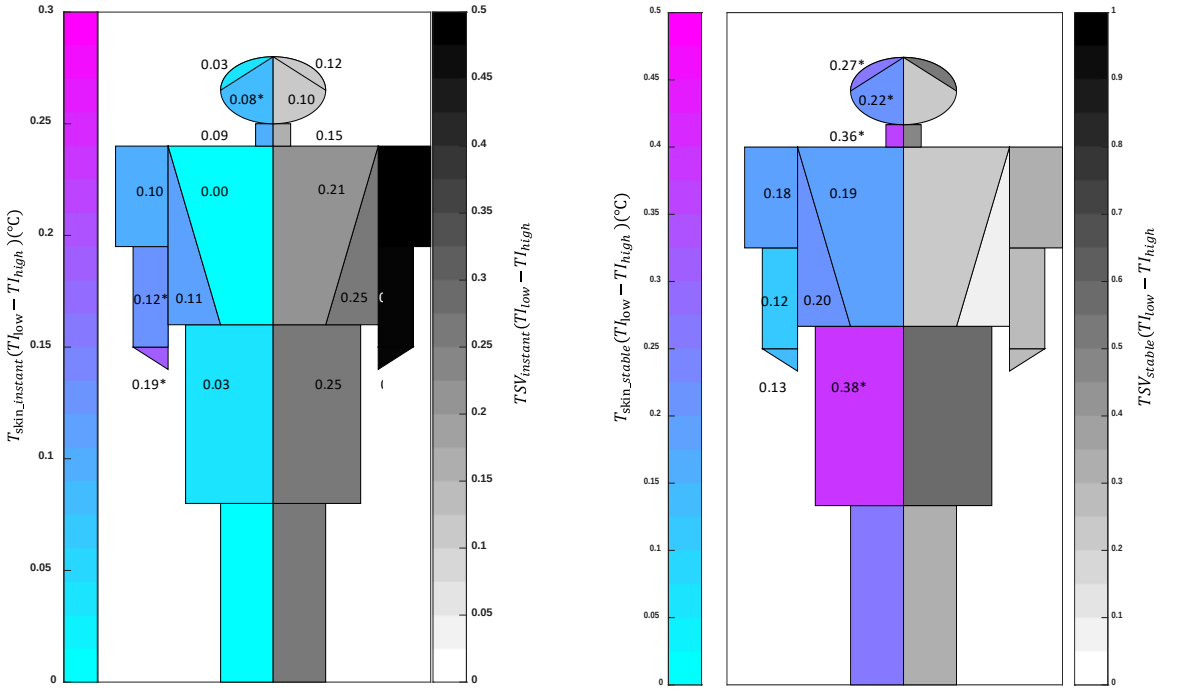

(c) Condition C

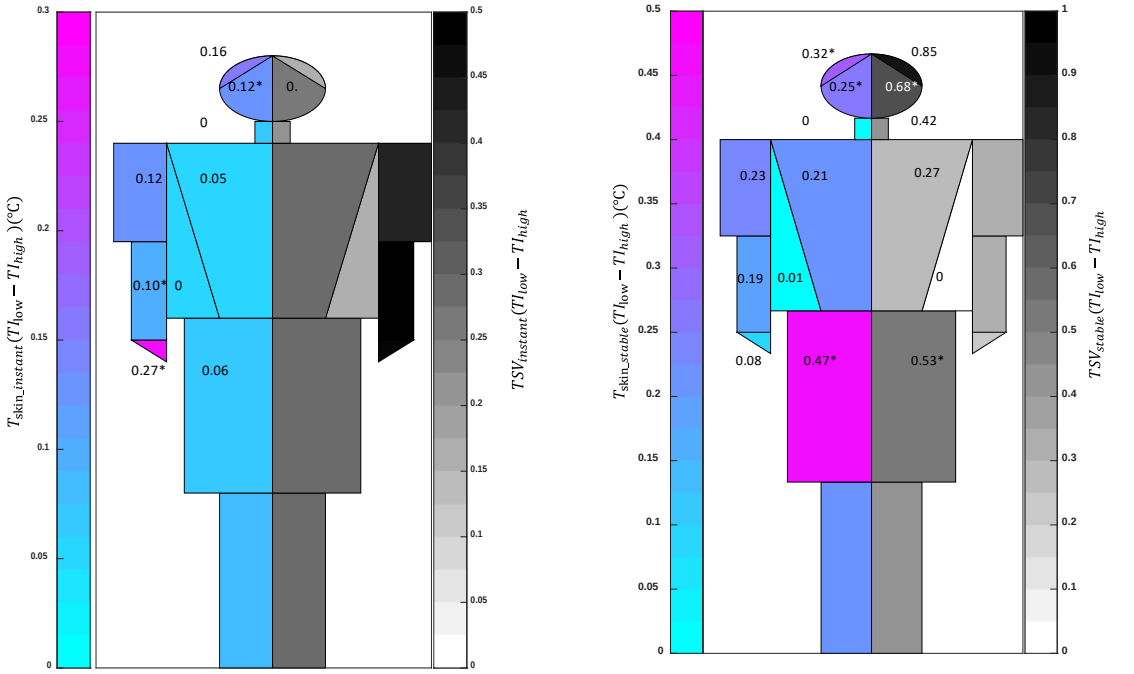

(d) Condition D

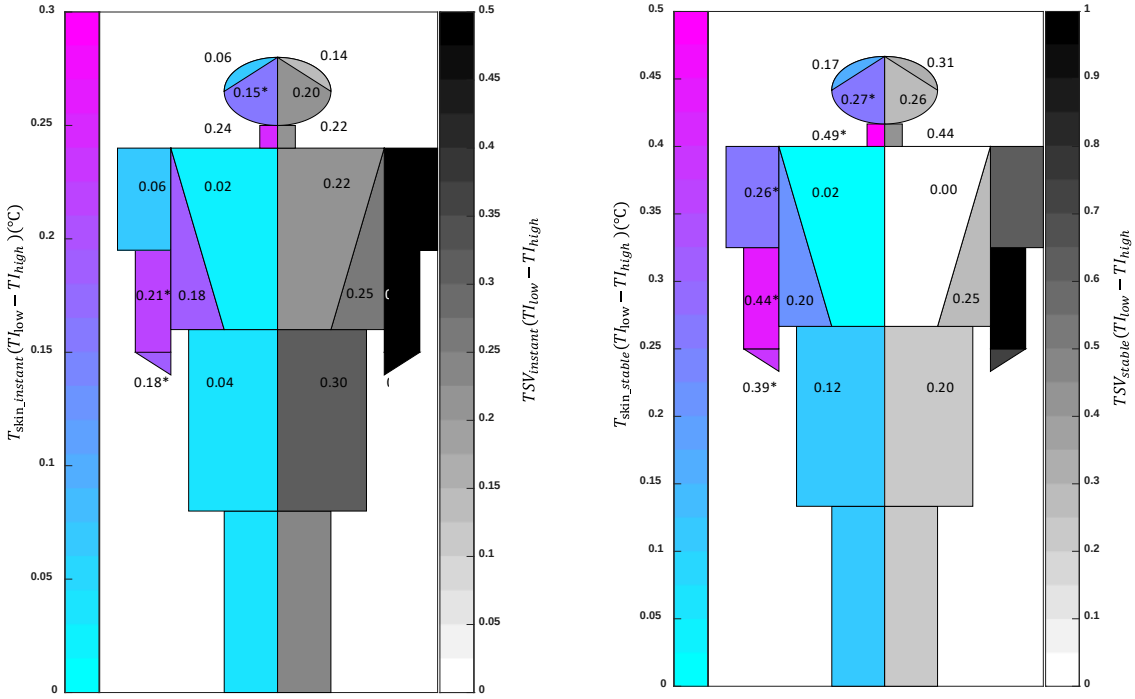

Fig.4. (a)-(d) body maps showing the regional distribution of turbulence-induced local skin temperature and thermal sensation difference for test conditions A through D (defined in Table 2). $T_{skin\_instant}(TI_{low} - TI_{high})$ and $TSV_{instant}(TI_{low} - TI_{high})$ refer to the instantaneous skin temperature and thermal sensation vote change between the two turbulence intensity levels; $T_{skin\_stable}(TI_{low} - TI_{high})$ and $TSV_{stable}(TI_{low} - TI_{high})$ refer to the stable state skin temperature thermal sensation vote change between the two turbulence intensity levels respectively. Statistically significant differences (t-test, $p<0.05$) are indicated with *.

3.2.2 Skin temperature fluctuation

The skin temperature fluctuated around a generally downward trend (as the most obvious example circled in Fig. 3b), probably a result of the anticipatory control encoded in the human thermoregulatory system (Brück, 1989). For example, our body increases heat production to cope with a sudden cold draught, and when the draught is removed, the extra heat will lead to an increase in skin temperature. Due to the lack of evidence to support the detachment of skin temperature fluctuation from the long-term decrease trend, we are not able to calculate the real-time fluctuation amplitude and frequency. Instead, we use the percentage of the negative skin temperature change rate ($PN\ \mathrm{dT_{skin}}$) to quantify the skin temperature fluctuation throughout the process (Equation 7).

$$PN\ \mathrm{dT_{skin}} = \sum \left| \frac{\mathrm{dT_{skin}}}{\mathrm{dt}} < 0 \right| / \sum \left| \frac{\mathrm{dT_{skin}}}{\mathrm{dt}} \right| \quad (7)$$

Where $\frac{\mathrm{dT_{skin}}}{\mathrm{dt}}$ $(°\mathrm{C}/\mathrm{s})$ is the rate of change of skin temperature. larger $PN\ \mathrm{dT_{skin}}$ indicates a more consistent skin temperature decrease with less rebound. The difference in $PN\ \mathrm{dT_{skin}}$ is maily evident in distal body segments when participants were standing side-on to the wind direction. For the cycling subjects' body segments in motion (thigh and shin), the fluctuation difference in local skin temperature overlapped with its decrement, and therefore the correlation between the turbulence-induced skin temperature fluctuation and the thermal sensation cannot be established. For the upper body parts, though local skin temperatures decreased with less fluctuation in the higher *TI* conditions, no corresponding difference in local thermal sensation was detected.

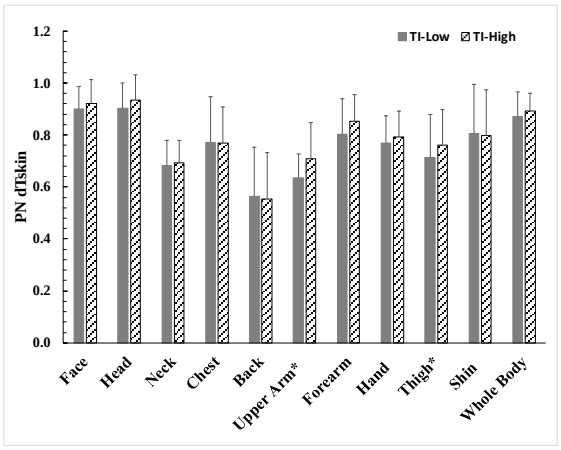

(a) Condition A

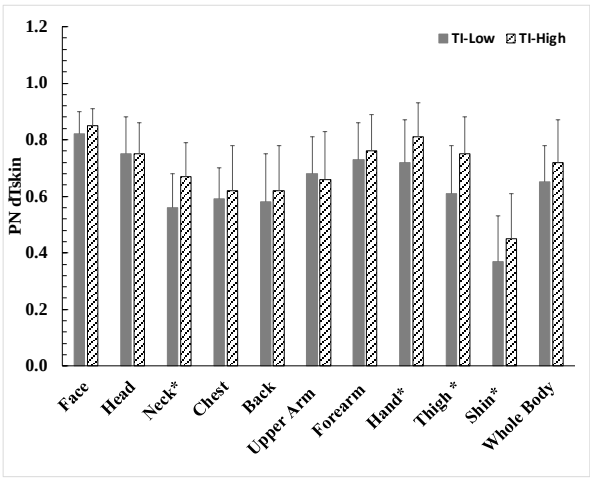

(b) Condition B

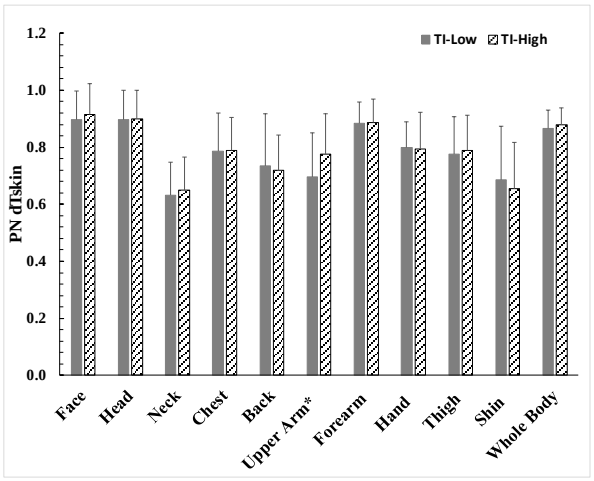

(c) Condition C

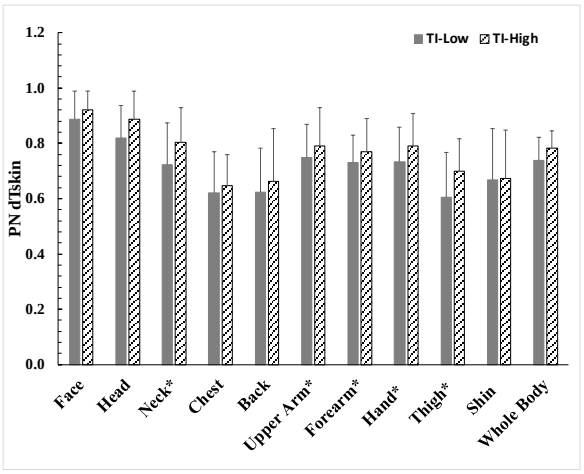

(d) Condition D

*significant difference ($P < 0.05$) between two turbulence intensity levels

Fig. 5. (a)-(d) Percentage of negative skin temperature change rate (mean ± standard deviation) for test conditions A to D.

3.3 Incorporating the effects of turbulence intensity in thermophysiological model

The above results prompt us to incorporate turbulence intensity into a contemporary thermal regulation model so that they may more accurately predict of skin temperature. We here use Gagge's 2-node thermophysiological model (Gagge, 1971) as an example (see its basic framework in Appendix A). It represents the human body as concentric cylinders - core and skin. The heat and mass transfer between the clothing and the skin is simplified by introducing a 'clothing thermal efficiency' factor.

The convective heat transfer coefficient (h_c) adopted in the current generation of thermophysiological models (Fiala et al., 2012; Fiala et al., 1999; Huizenga et al., 2001b; Tanabe et al., 2002) shared a similar form as,

$$h_c = a * v^b \tag{8}$$

where, v is the air velocity, *a* and *b* are coefficients, set to 8.6 and 0.53 (Doherty & Arens, 1988).

Accounting for the effect of both wind velocity and turbulence intensity, an updated convective heat transfer coefficient equation generated from our previous experiment is given as,

$$h_c = A * v^n * (1 + B * TI * v^{0.5}), \quad (9)$$

where, v is the air velocity, *TI* is turbulence intensity, A, B, and n are coefficients, set to 9.93, 1.03, and 0.54 respectively for estimating the whole-body convective heat loss (Yu et. Al., 2020). Considering that only the wind velocity can be used as the model input, we reverse calculated the "equivalent velocity (v_{equal})" as ,

$$v_{equal} = \sqrt[b]{\frac{A*v^n*(1+B*TI*v^{0.5})}{a}} \quad (10)$$

For cycling conditions (**B** and **C)**, heat was continuously generated by the metabolic process, initiating regulatory sweating for thermal regulation. Areal distribution of sweating reported in previous research (Valenza et al., 2019) suggests that among the body segments directly exposed to the wind, forehead, thigh, and shin have higher-than-average sweat rates. Given that the evaporative heat transfer coefficient is 2.2 times the convective heat transfer coefficient (Equation 15), the pronounced difference in skin temperature reduction and cooling sensation on these body parts at two turbulence levels can then been explained (Fig.4 b-c).

The open-source R Package -"calc2Node" (Schweiker et al., 2019), translated from Fountain and Huizenga (Fountain & Huizenga, 1997) implementation of Gagge's 2-Node model (Gagge et al., 1971), was used to iterate the skin and core temperature over time. The model outputs the body mean skin temperature results every one minute. Considering that Gagge's 2-node model does not distinguish the local differences inside the skin and core shells, which means the difference in wind direction can't be reflected in the model's output, we here only compared both wind-facing conditions **A** and **C**.

Fig.6 shows that the modified 2 node model accounting for the effects of both wind velocity and turbulence intensity is able to distinguish skin temperature responses for the two turbulence levels. The unmodified 2 node model underestimates the cooling effect of wind by more than 30% for the standing condition (**A**), and 50% for the cycling condition (**C**). However, it should be clarified that these underestimations were not entirely caused by the overlook of turbulence intensity in equation (8). Although equations (8) and (9) were both generated from the manikin experiment, the size, posture, and the operation mode of the thermal manikin unavoidably led to the difference in its coefficients that act on air velocity. Within the velocity range specified in Table 2, when we set TI in equation (9) to zero, the predicted convective heat transfer coefficient is around 16% larger than the result from equation (8).

In the two node model, the human body is considered as a single segment on which clothing insulation and evaporative sweating are regarded as evenly distributed over the entire skin surface. This gross simplification inevitably underestimates the fast response of those body segments directly exposed to airflow, e.g. head and extremities. Therefore, we believe that applying this updated convective heat transfer coefficient in a multi-segment thermal regulation model will further improve predictive skill under a complex real outdoor environments.

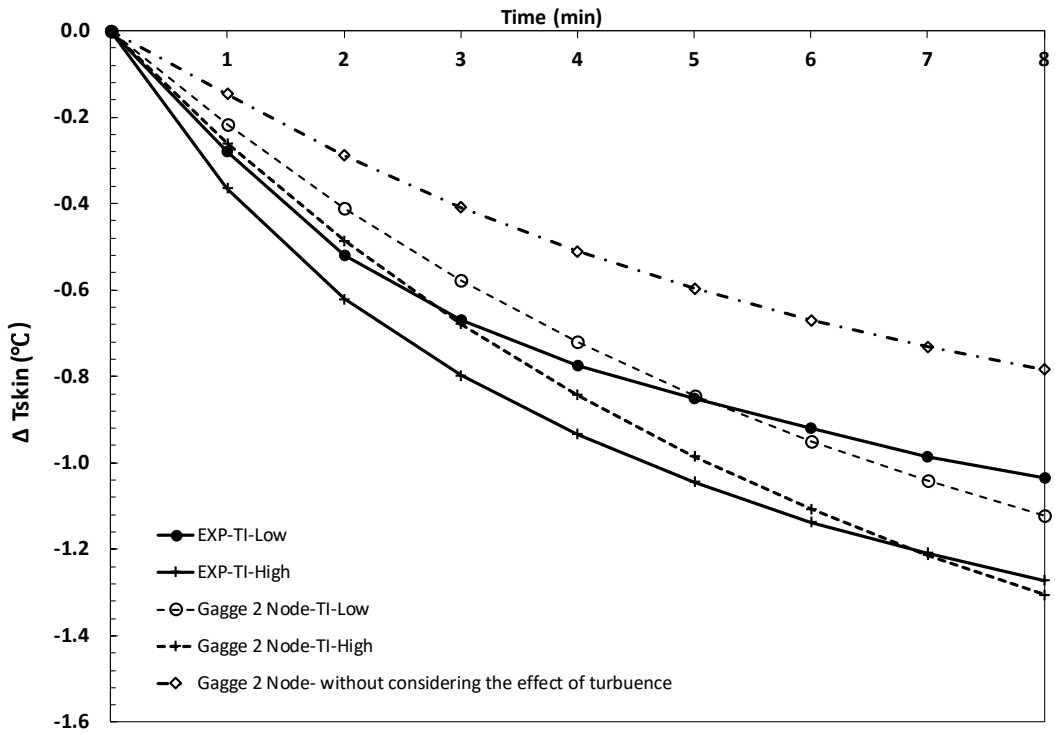

Condition **A**

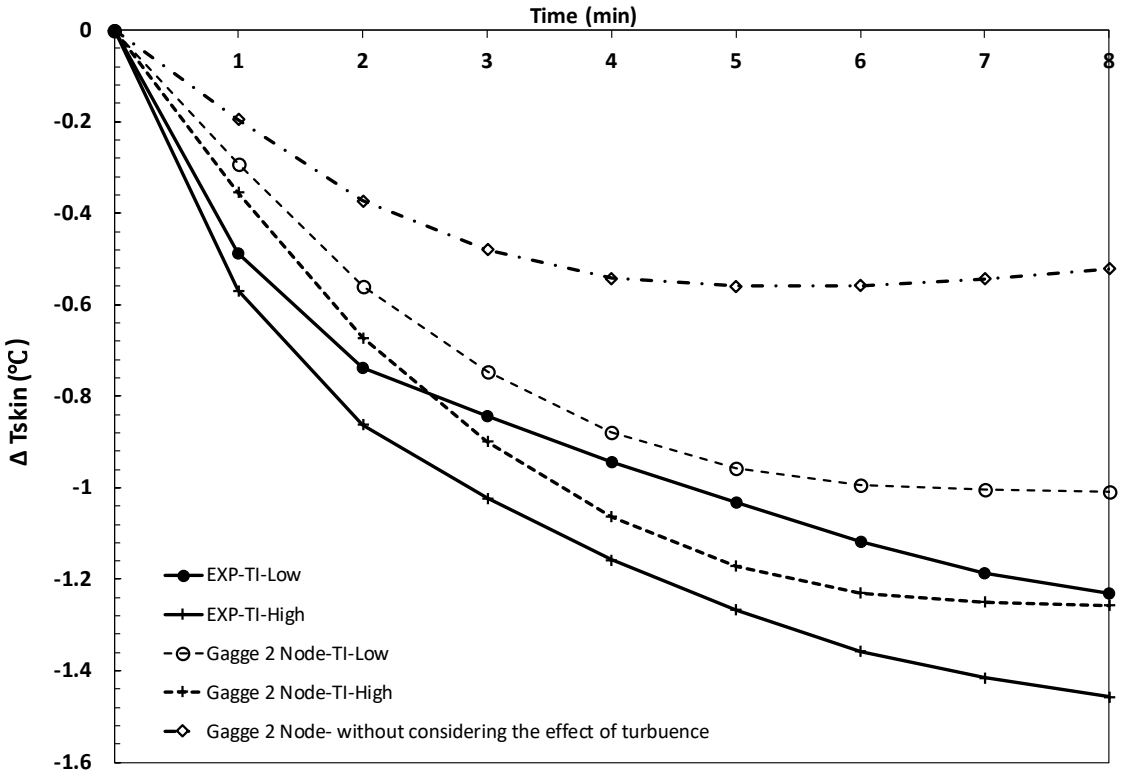

Condition **C**

Fig.6. The comparison of whole-body mean skin temperature change at different turbulence levels ("circle" represents *TI*-low, "cross" represents *TI*-high) between the experiment result (solid lines) and Gagge's two-node model output (dash line); the dash-dot line is the original model output which did not consider the effect of turbulence.

3.4 Clarifying the instantaneous response to turbulence intensity in the thermoreceptor model

As seen in Fig. 6, the shortest calculation time-step in the up-to-date thermal comfort models was 1-min, which may be fast enough to simulate the thermal response under a steady-state condition, but is not suitable for a transient condition. A gust of wind, for example, which usually lasting for less than 20 seconds (Oke, 1987), will be weakened when averaged over a one-minute period for the purposes of calculation. Besides, this one-minute calculation time step also overlooks our ability to instantly perceive thermal transients. The neurons that sense these distinct stimuli, known as cold and warm thermoreceptors, are located at 0.2 mm and 0.5 mm below the skin surface. The potential signal transformed through afferent fibres to hypothalamus at a speed of 10-20 m/s and 1-2 m/s, for the cold and warm receptors, respectively (Hensel & Schafer, 1984).

Hensel et al. (Hensel & Schafer, 1984) have demonstrated that the thermal response of cutaneous thermoreceptor is influenced by the local temperature and its rate of change. According to this, de dear et al. (de Dear et al., 1993) developed a cutaneous thermoreceptor model to simulate the heat diffusion through clothing and skin layers under transient thermal stimuli, and correlated the temperature and its change rate at the depth of cold and warm thermoreceptors with the impulse frequency. Subsequent human subject experiments demonstrated that the magnitude of thermal sensation response to the step changes in air temperature and metabolic rate was proportional to the cumulative thermal receptor impulses during the first 20 s (Ring & de Dear, 1991).

We simulated the thermal response of cutaneous thermoreceptor (see the details in Appendix B) of condition **A** (Fig. 7), including the time-variant temperature in cold receptor and the corresponding cutaneous thermoreceptor impulses multiplied by the Area Summation Factor for both exposed and clothed skin.

At the end of the 20 s, the skin temperature difference in cold receptors between the two turbulence intensity levels in the exposed skin area is 0.09 ℃, which matched well with the experimental observation (0.12 ℃) reported in Table 4. The overshoot phenomenon is more pronounced for the uncovered body parts, and accounts for most (~80%) of the total impulse rate at the cold thermoreceptor. *DTS* calculations came to 273 and 225 impulses for the high and low *TI* simulations respectively. Given the relationship between the thermal sensation vote (*TSV*) and dynamic thermal stimulus (*DTS*) was approximated as $TSV=0.01*DTS$ in ref (de Dear et al., 1993), the *DTS* difference of 48 impulses translates into a 0.5 unit difference on the 7-point *TSV* rating scale, which matches well with our experimental observations for condition **A** in Table 3.

In this experiment, all the participants started the test from a neutral thermal sensation. But the cooling effect of wind for a warm-to-hot thermal discomfort zone is probably of more practical interest. To calculate the temperature distribution within body tissue when the subjects is in a non-neutral thermal status, Lv & Liu (2007) replaced the original finite difference model (de Dear et al., 1993) with the well known Pennes equation (Pennes, 1948), which includes the effects of metabolism and blood perfusion on the energy balance of tissue. Later, Zolfaghari et al. (Zolfaghari & Maerefat, 2010) replaced the fixed inner body temperature in Pennes equation with the time-dependent blood and core temperature output from Gagge's 2-node model. However, the coefficient K_s and K_d are related to the initial adaptive temperature, and the area summation factors (*ASF*) may vary with different stimulus types and clothing insulation (Hensel & Schafer, 1984). To further extend the model for transient environmental and metaboloic applications, more extensive experimental work with human subjects would be

valuable in providing an empirical basis for the various coefficients in the perceptual postprocessing of simulated cutaneous thermoreceptor outputs.

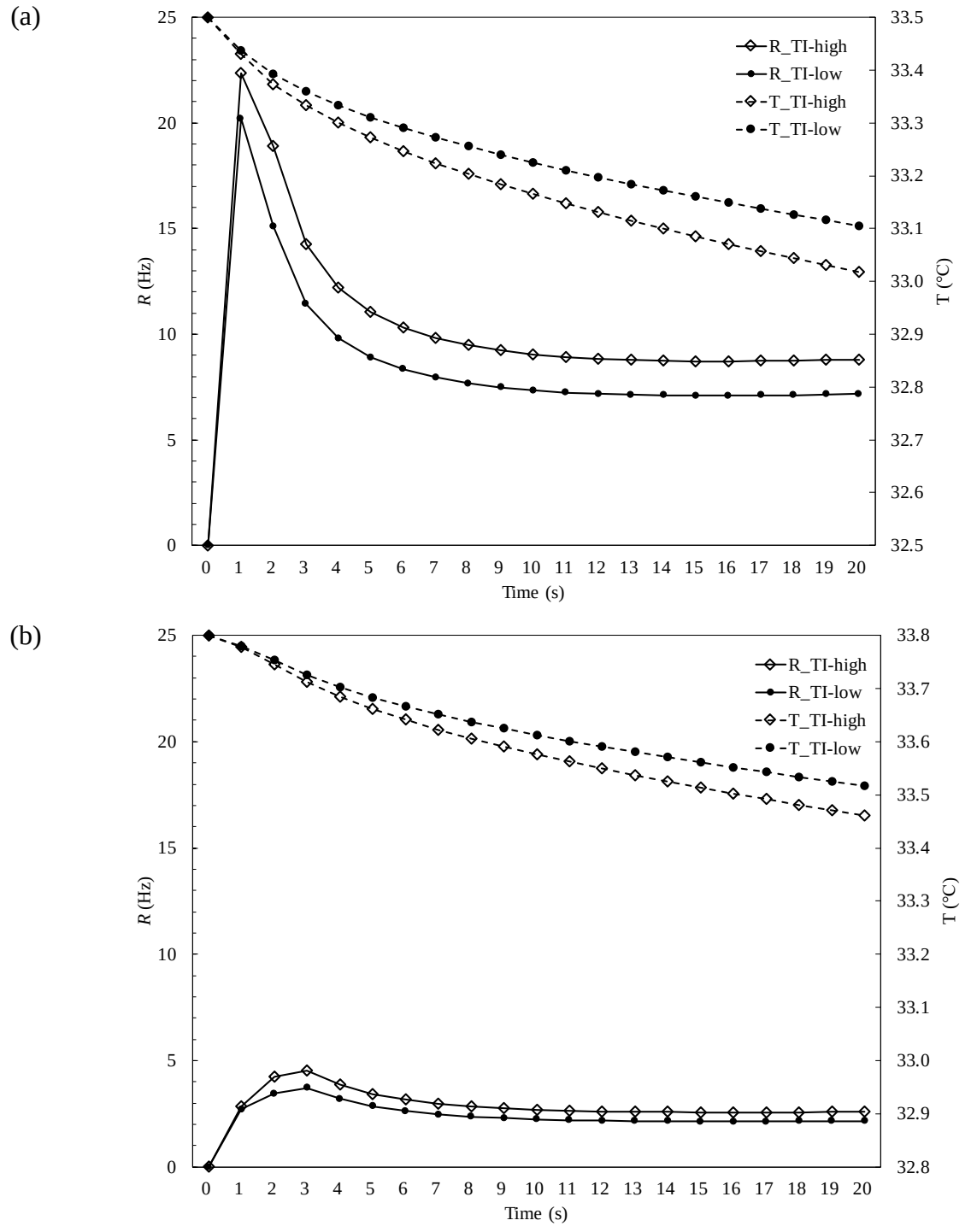

Fig. 7. Temperature and impulses at cold cutaneous thermoreceptors in (a) exposed and (b) clothed skin sites, in the first 20 s after the thermal transient for two turbulence levels.

4. Conclusions

This study confirms the impact of turbulence-induced cooling on both physiological and perceptual responses of human subjects to wind. When directly facing the wind, the subjects could almost instantly feel the difference between two levels of turbulence intensity (35% and 17%), which was reflected by the proportional change of skin temperature. The mean skin temperature difference between two turbulence levels continues to increase, and reached statistically significant after 10-min under all test conditions, while the difference in sensation was only perceptible under the cycling conditions, at which the higher turbulence intensity amplified not only the convective heat loss but also the evaporation of sweat, causing cooler sensation in these active parts of the body.

Equipped with the updated convective heat transfer coefficient to account for the effects of both wind velocity and turbulence intensity, previously published models of skin thermorecepetor and the physiological thermoregulation are now more accurate in simulating both instantaneous and steady-state thermal physiological response under dynamic wind exposures. Ignoring the turbulence intensity may underestimate the mean skin temperature decrement by 14% and 34% for standing and cycling conditions respectively. Therefore, "Equivalent velocity" should replace the "mean velocity" as one of the environmental inputs of the thermal comfort model to account for the effect of turbulence intensity in outdoor thermal comfort studies.

In this study, all the participants wore typical summer clothing and started each test with a neutral thermal sensation. We are not able to conclude the cross-impact between air temperature, humidity, and turbulence intensity on the thermal perception. Future studies using computational simulation (Ono et al., 2008; Zou et al., 2020) or wind tunnel testing require a broader test range so as to cover typical outdoor environmental conditions, and to investigate the cross-impact of air temperature, humidity, and turbulence intensity on the thermal perception. Besides, it is also important to validate these experimental findings in real outdoor scenarios, paying particular attention to the relative motion when the pedestrians are moving (Mochida & Lun, 2008).

5. Conflict of interest

The authors declare that there is no conflict of interest.

6. Acknowledgement

This research was supported by the School of Architecture, Design and Planning, and the School of Civil Engineering, both at The University of Sydney. The authors wish to thank Mr Zachary Benitez, Mr Theo Gresley-Daines, and Mr Jiwei Zou for their technical support and assistance with the wind tunnel experiments.

Appendix A. The basic framework of Gagge's 2-node thermophysiological model

Heat storage (St) in the system consists of heat production in the body core (including metabolic rate (M) and shivering (Mshiv)) minus the heat transferred between skin surface and the surrounding environment. These transfers include respiration (Qres), skin evaporation (Esk), radiative heat loss (Qr), and convective heat loss (Qc)):

St=M+Mshiv -Qres-Qc-Qr-Esk (A.1)

The heat transfer occurs between core and skin (Q_{cs}) through direct conduction and blood flow can be written as,

$$Q_{cs} = A_D(K + Cbl * Vb) * (T_{cr} - T_{sk}) \quad (A.2)$$

Where K ($W/m^2℃$) is the effective conductance between core and skin; A_D (m^2) is the body surface area; Cbl (W hr/kg ℃) is the specific heat of blood; Vb ($kg/hr\ m^2$) is the mass blood flow between core and skin.

and the rate of heat storage in the skin (Ssk) and core (Scr) can be expressed as:

$$Ssk = \alpha * m * Cb * dT_{skin}/dt \quad (A.3)$$

$$Scr = (1 - \alpha) * m * Cb * dT_{cr}/dt \quad (A.4)$$

where α is the skin shell's fraction of body mass, usually set as 0.1; m (kg) is the mass of the whole body; Cb is the specific heat of the body (0.97 W hr/kg ℃). Equation (A.1) can be rewrittened as:

$$m * Cb * [\alpha * dT_{skin}/dt + (1 - \alpha) * dT_{cr}/dt] = M+Mshiv -Qres-Qc-Qr-Esk \quad (A.5)$$

Among those heat balance components on the right side of the Equation (A.1), convective and evaporative heat loss from the skin surface are directly determined by the convective heat transfer coefficient (h_c), as follows:

$$Q_c = A_D * fcl * (T_{cl} - T_a) * h_c \quad (A.6)$$

$$Esk = (0.06 + 0.094 * wrsw) * A_D * fcl * (Pcl - Pa) * h_e \quad (A.7)$$

Where,

fcl is the ratio of clothed body surface area to nude body surface area, and estimated on the basis of the amount of thermal insulation being worn by the subject. In this 2-node model (Gagge et al., 1971) the fcl estimation is expressed as $(1 + 0.15 * clo)$, and clo is the amount of intrinsic clothing thermal insulation, with 1 clo representing 0.155 m^2 ºC W^{-1} (ASHRAE, 2017),

T_{cl} (℃) is the clothing temperature,

T_a (℃) is the air temperature,

Wrsw is the fractional skin area covered by regulatory sweat,

Pcl (mm Hg) is the saturated vapor pressure at the clothing surface temperature,

Pa (mm Hg) is the partial vapor pressure of ambient air,
h_e $(W/m^2/K)$ is the evaporative heat transfer coefficient usually set as $2.2 * h_c$.

Appendix B. The basic framework of a simulated numerical skin thermoreceptor model

We replicated the clothing and skin model with the configuration and specific coefficient listed in Fig. B.1. and Table B.1 (Ring & de Dear, 1991; Zolfaghari & Maerefat, 2010).

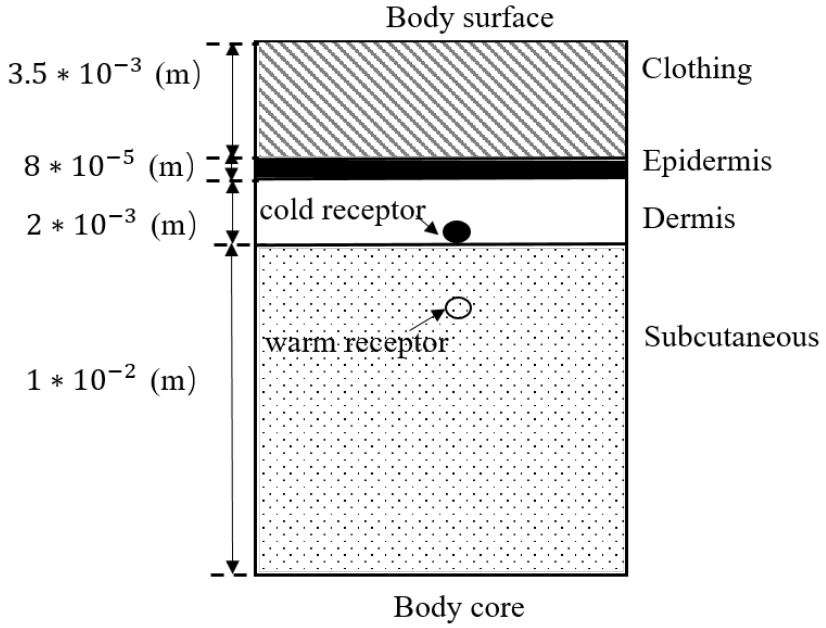

Fig. B.1. The physical configuration of clothing and skin model

Table B.1 Geometry and properties of the skin.

Location	Property		
	Thermal conductivity **k** (W/m K)	Specific heat **C** (J/kg/K)	Mass density **ρ** (kg/m^3)
Clothing	0.35	1380	31.7
Epidermis	0.24	3600	1200
Dermis	0.45	3400	1200
Subcutaneous	0.19	3060	1000

For the boundary conditions, the temperature at the body core was set to 36.8 ℃, the ambient temperature at the skin surface was set to 27 ℃, which is the average value during the experiment, and the radiant temperature was considered the same with the air temperature. The time-dependent temperature of skin tissue was obtained by solving

$$\rho * C * \frac{\partial T(x,t)}{\partial x} = k * \frac{\partial^2 T(x,t)}{\partial x^2} \quad \text{(B.1)}$$

Where,

$T(x, t)$ (℃) is the tissue temperature,

x (m) is the depth of the tissue (x=0 at the body core).

The convective-radiative boundary condition at the skin surface and a constant temperature at body core was set as:

$$-k * \frac{\partial T}{\partial x} = h_c * (T - T_a) + \sigma * \varepsilon * ((T + 273)^4 - (T_a + 273)^4) \quad \text{at skin surface (B.2)}$$

$T=T_{cr}$ at body core (B.3)

Where

σ is the Stefan-Bolzmann constant ($5.67*10^{-8}$ W/m^2 k^4),

ε is the body surface emissivity (set to 0.9 for clothing and skin surface in this study).

The model was first iterated for the initial temperature distribution with a neutral convective heat transfer coefficient ($h_c = 3.4$ W/m^2/K) at t = 0 s. The initial temperature (also known as adaptive temperature) at the cold receptor was 33.5 ℃ and 33.8 ℃ for unclothed and clothed conditions, respectively. The cutaneous thermoreceptor impulse frequency R at two turbulence levels with different h_c (Equation 9) was calculated with a time-step of 0.05 s as

$$R(\text{cold}) = \begin{cases} K_s T_{(x,t)} & \frac{\partial T}{\partial t} > 0 \\ K_s T_{(x,t)} + K_d \frac{\partial T}{\partial t}, & \frac{\partial T}{\partial t} < 0 \end{cases} \quad \text{(B.4)}$$

$$R(\text{warm}) = \begin{cases} K_s T_{(x,t)}, & \frac{\partial T}{\partial t} < 0 \\ K_s T_{(x,t)} + K_d \frac{\partial T}{\partial t}, & \frac{\partial T}{\partial t} > 0 \end{cases} \quad \text{(B.5)}$$

Where,

$R\ (cold)$is the impulse frequency elicited by cold thermoreceptor,

$R\ (warm)$is the impulse frequency elicited by warm thermoreceptor,

K_s is the proportional coefficient for static discharge, set as +2 for warm receptor and -2 for cold receptor,

K_d is the proportional coefficient for dynamic discharge, set as +56 for warm thermoreceptor and -62 for cold receptor,

T is the temperature at the receptor site.

We calculated the whole-body Dynamic Thermal Stimulus (*DTS*) which integrated the sum of all impulses accumulated from local skin regions (de Dear et al., 1993), to connect thermoreceptor impulse rate to thermal sensation, with this function:

$$DTS = \sum_{t=1}^{20}(ASF * R_t) \quad \text{(B.6)}$$

Where,

ASF is the "Area Summation Factor": in the exposed skin aera, *ASF* is set as 5 for both cold and warm thermoreceptors, while in the clothed skin area, *ASF* is set as 2 for cold thermoreceptors and and 1 for warm thermoreceptors, respectively;

R_t is the impulse frequency for individual body parts at time *t* (s), calculated using Equation (B.4)-(B.5).

Since only cold receptors respond to the down-step skin temperature changes, Equation (B.6) can be rewritten as,

$$DTS = \sum_{t=1}^{20}(2 * R(\text{clothed})_{(t)} + 5 * R(\text{exposed})_{(t)}) \quad \text{(B.7)}$$

References

ASHRAE. (2017). *ASHRAE handbook: Fundamentals*. American Society of Heating, Refrigerating and Air-Conditioning Engineers.

Asimakopoulus, D., & Santamouris, M. (2012). *Energy and climate in the urban built environment*: Routledge. doi: https://doi.org/10.4324/9781315073774

Assimakopoulos, V. D., ApSimon, H. M., & Moussiopoulos, N. (2003). A numerical study of atmospheric pollutant dispersion in different two-dimensional street canyon configurations. Atmospheric Environment, 37(29), 4037-4049.

Brück, K. (1989). Thermal balance and the regulation of body temperature. In R. F. Schmidt & G. Thews (Eds.), *Human Physiology* (pp. 624-644). Springer Berlin Heidelberg.

Crouter, S. E., Albright, C., & Bassett, D. R. (2004). Accuracy of polar S410 heart rate monitor to estimate energy cost of exercise. Medicine and Science in Sports and Exercise, 36, 1433-1439.

Darian-Smith, I., & Johnson, K. O. (1977). Thermal sensibility and thermoreceptors. *Journal of Investigative Dermatology, 69*(1), 146-153. doi:https://doi.org/10.1111/1523-1747.ep12497936

de Dear, R., Ring, J. W., & Fanger, P. O. (1993). Thermal Sensations Resulting From Sudden Ambient Temperature Changes. *Indoor Air, 3*(3), 181-192. doi:10.1111/j.1600-0668.1993.t01-1-00004.x

Doherty, T., & Arens, E. (1988). Evaluation of the physiological bases of thermal comfort models. *ASHRAE Trans, 94*.

Fanger, P. O., Melikov, A. K., Hanzawa, H., & Ring, J. (1988). Air turbulence and sensation of draught. *Energy and Buildings, 12*(1), 21-39. doi:https://doi.org/10.1016/0378-7788(88)90053-9

Fiala, D., Havenith, G., Bröde, P., Kampmann, B., & Jendritzky, G. (2012). UTCI-Fiala multi-node model of human heat transfer and temperature regulation. *International Journal of Biometeorology, 56*(3), 429-441. doi:10.1007/s00484-011-0424-7

Fiala, D., Lomas, K., & Stohrer, M. (1999). A computer model of human thermoregulation for a wide range of environmental conditions: The passive system. *Journal of Applied Physiology, 87*(5), 1957-1972.

Fountain, M., & Huizenga, C. (1997). A thermal sensation prediction software tool for use by the profession. *ASHRAE Trans, 103*, 130-136.

Gagge, A. P., Stolwijk, J., & Nishi, Y. (1971). An effective temperature scale based on a simple model of human physiological regulatory response. *ASHRAE Trans., 77*, 247-262. Retrieved from https://ci.nii.ac.jp/naid/10003090056/en/

Gagge, A. P., & Nishi, Y. (1977). Heat exchange between human skin surface and thermal environment. In*Comprehensive Physiology, S26 Handbook of physiology, reactions to environmental agents (*pp. 69-92).

Givoni, B., & Goldman, R. F. (1972). Predicting rectal temperature response to work, environment, and clothing. *Journal of Applied Physiology, 32*(6), 812-822. doi:10.1152/jappl.1972.32.6.812

Godbey, G. (2009). Outdoor Recreation, Health, and Wellness: Understanding and Enhancing the Relationship. *SSRN Electronic Journal, RFF Discussion* Paper No. 09-21. doi:10.2139/ssrn.1408694

Griefahn, B., Künemund, C., & Gehring, U. (2000). The significance of air velocity and turbulence intensity for responses to horizontal drafts in a constant air temperature

of 23°C. *International Journal of Industrial Ergonomics, 26*(6), 639-649. doi:https://doi.org/10.1016/S0169-8141(00)00033-0
Hensel, H., & Schafer, K. (1984). Thermoreception and temperature regulation in man T. In E. F. J. Ring & B. Phillips (Eds.), *Recent advances in medical thermology* (pp. 51-64). Springer.
Hogg, R. V., Tanis, E. A., & Zimmerman, D. L. (2010). Probability and statistical inference. In (pp. 355-415). Pearson/Prentice Hall.
Huang, L., Ouyang, Q., & Zhu, Y. (2012). Perceptible airflow fluctuation frequency and human thermal response. *Building and Environment, 54*, 14–19. doi:10.1016/j.buildenv.2012.02.004
Huizenga, C., Hui, Z., & Arens, E. (2001a). A model of human physiology and comfort for assessing complex thermal environments. *Building and Environment, 36*(6), 691-699. doi:https://doi.org/10.1016/S0360-1323(00)00061-5
Kingma, B. R. M. (2012). Human thermoregulation: A synergy between physiology and mathematical modelling (Doctoral dissertation, Maastricht University, Maastricht, England).
Kingma, B. M. R., Schellen, L., Frijns, A. J. H., & van Marken Lichtenbelt, W. D. (2012). Thermal sensation: A mathematical model based on neurophysiology. *Indoor Air, 22*(3), 253–262.
Lin, T.P., Tsai, K.T., Liao, C.C., & Huang, Y.C. (2013). Effects of thermal comfort and adaptation on park attendance regarding different shading levels and activity types. *Building and Environment, 59*, 599-611. doi:https://doi.org/10.1016/j.buildenv.2012.10.005
Lv, Y., & Liu, J. (2007). Effect of transient temperature on thermoreceptor response and thermal sensation. *Building and Environment, 42*, 656-664. doi:10.1016/j.buildenv.2005.10.030
Mayer, E. (1987). Physical causes for draft: some new findings. *ASHRAE Trans, 93*, 540-548.
Mochida, A., & Lun, I. Y. (2008). Prediction of wind environment and thermal comfort at pedestrian level in urban area. Journal of wind engineering and industrial aerodynamics, 96(10-11), 1498-1527.
Niachou, K., Livada, I., & Santamouris, M. (2008). Experimental study of temperature and airflow distribution inside an urban street canyon during hot summer weather conditions. Part II: Airflow analysis. Building and environment, 43(8), 1393-1403.
Oke, T. R. (1987). *Boundary Layer Climates* (2nd ed.). Lagos: Routledge.
Ono, T., Murakami, S., Ooka, R., & Omori, T. (2008). Numerical and experimental study on convective heat transfer of the human body in the outdoor environment. Journal of Wind Engineering and Industrial Aerodynamics, 96(10-11), 1719-1732.
Parkinson, T., & de Dear, R. (2016). Thermal pleasure in built environments: Spatial alliesthesia from air movement. *Building Research & Information, 45*, 1-16. doi:10.1080/09613218.2016.1140932
Pennes, H. (1948). Analysis of tissue and arterial blood temperatures in the resting human forearm. *Journal of Applied Physiology, 1*(2), 93-122. doi:10.1152/jappl.1948.1.2.93
Ring, J. W., & de Dear, R. (1991). Temperature transients: A model for heat diffusion through the skin, thermoreceptor response and thermal sensation. *Indoor Air, 1*(4), 448-456. doi:10.1111/j.1600-0668.1991.00009.x

Scaperdas, A., & Colvile, R. N. (1999). Assessing the representativeness of monitoring data from an urban intersection site in central London, UK. Atmospheric Environment, 33(4), 661-674.

Schweiker, M., Mueller, S., Kleber, M., Kingma, B., & Shukuya, M. (2019). *Functions for thermal comfort research.* R Package Version 0.1.9.

Stathopoulos, T. (2006). Pedestrian level winds and outdoor human comfort. Journal of wind engineering and industrial aerodynamics, 94(11), 769-780.

Stolwijk, J. A. J. (1971). *A mathematical model of physiological temperature regulation in man*. NASA-CR-1855, CONTRACT_GRANT: NAS9-9531.

Tanabe, S., Kobayashi, K., & Nakano, J. (2002). Evaluation of thermal comfort using combined multi-node thermoregulation (65MN) and radiation models and computational fluid dynamics (CFD). *Energy & Buildings, 34*(6), 637-646.

Tanabe, S., & Kimura, K. (1989). Importance of air movement for thermal comfort under hot and humid conditions. *Proceedings of the Second ASHRAE Far East Conference on Air Conditioning in Hot Climates*, 95-103.

Valenza, A., Bianco, A., & Filingeri, D. (2019). Thermosensory mapping of skin wetness sensitivity across the body of young males and females at rest and following maximal incremental running. *The Journal of Physiology, 597*(13), 3315-3332. doi:10.1113/jp277928

Wang, Y., Lian, Z., & Lan, L. (2011). The effect of turbulence intensity on local skin temperature and subjective responses to draft. *Energy and Buildings, 43*(10), 2678-2683. doi:https://doi.org/10.1016/j.enbuild.2011.06.021

Xia, Y. Z., Niu, J. L., Zhao, R. Y., & Burnett, J. (2000). Effects of turbulent air on human thermal sensations in a warm isothermal environment. *Indoor Air, 10*(4), 289-296. doi:10.1034/j.1600-0668.2000.010004289.x

Xie, Y., Huang, T., Li, J., Liu, J., Niu, J., Mak, C. M., & Lin, Z. (2018). Evaluation of a multi-nodal thermal regulation model for assessment of outdoor thermal comfort: Sensitivity to wind speed and solar radiation. *Building and Environment, 132*, 45-56. doi:https://doi.org/10.1016/j.buildenv.2018.01.025

Xie, Y., Niu, J., Zhang, H., Liu, S., Liu, J., Huang, T., . . . Mak, C. M. (2020). Development of a multi-nodal thermal regulation and comfort model for the outdoor environment assessment. *Building and Environment, 176*, 106809. doi:https://doi.org/10.1016/j.buildenv.2020.106809

Yokota, M., Berglund, L., Cheuvront, S., Santee, W., Latzka, W., Montain, S., . . . Moran, D. (2008). Thermoregulatory model to predict physiological status from ambient environment and heart rate. *Computers in Biology and Medicine, 38*(11-12), 1187.

Yu, Y., Liu, J., Chauhan, K., de Dear, R., & Niu, J. (2020). Experimental study on convective heat transfer coefficients for the human body exposed to turbulent wind conditions. *Building and Environment, 169*, 106533. doi:https://doi.org/10.1016/j.buildenv.2019.106533

Zhang, H., Huizenga, C., Arens, E., & Yu, T. (2001). Considering individual physiological differences in a human thermal model. *Journal of Thermal Biology, 26*(4–5), 401-408.

Zhao, R., Zhang, Y., Yu, N., & Di, H. (2006). Literature review of airflow fluid characteristics and their impact on human thermal comfort.

Zhou, X., Ouyang, Q., Lin, G., & Zhu, Y. (2010). Impact of dynamic airflow on human thermal response. *Indoor Air, 16*(5), 348-355.

Zolfaghari, A., & Maerefat, M. (2010). A new simplified thermoregulatory bioheat model for evaluating thermal response of the human body to transient environments. *Building and Environment, 45*(10), 2068-2076. doi:https://doi.org/10.1016/j.buildenv.2010.03.002

Zou, J., Liu, J., Niu, J., Yu, Y., & Lei, C. (2020). Convective heat loss from computational thermal manikin subject to outdoor wind environments. Building and Environment, 107469 .

Zou, J., Yu, Y., Liu, J., Niu, J., Chauhan, K., & Lei, C. (2021). Field measurement of the urban pedestrian level wind turbulence. Building and Environment, 194, 107713.